Building and Environment 218 (2022) 109111

Contents lists available at ScienceDirect

Building and Environment

journal homepage: www.elsevier.com/locate/buildenv

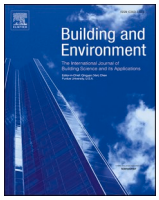

Automatic fault diagnosis algorithm for hot water pipes based on infrared thermal images

Hang Guan, Tong Xiao, Wei Luo, Jiefan Gu, Ruikai He, Peng Xu *

School of Mechanical and Energy Engineering, Tongji University, Shanghai, 201804, China

ARTICLE INFO

Keywords:
Water pipe
Fault diagnosis
Infrared thermal images
Computer vision
Image processing

ABSTRACT

In recent years, scholars have completed many studies on the fault diagnosis of air-conditioning systems based on Building Energy Management System (BEMS) data, but these studies seldom cover the leakage of water pipes and the damage of insulation layer, that are common but undetected by BEMS. To fill in the gaps, an automatic diagnosis algorithm based on infrared thermal images is proposed here to detect fault occurs on insulated heating pipes. This method can automatically diagnosis of pipeline leakage and insulation damage, so as to prevent pipeline corrosion and heat loss. The algorithm includes two sections: an image segmentation processor and a fault diagnosis module. The fault diagnosis module can detect three categories of faults: insulation damaged, insulation fall-off, and pipeline leakage. Experimental study demonstrates that the overall accuracy of the algorithm is 97.59%, while filed studies in commercial buildings exhibits an accuracy of 92.74%. These data prove the algorithm's feasibility in practice and the method can be applied with an infrared camera installed on an inspection robot or at a fixed location in a machine room. Although images of hot water pipes are used as inputs of the research, this method is also applicable to cold water pipes by modifying relevant parameters.

1. Introduction

The detection of building HVAC faults has been well studied since 1980s in order to ensure the efficient operation of HVAC system. Today, commercially available automated fault detection and diagnostics (FDD) tools are increasingly used in practice. Janghyun Kim et al. summary ranges of fault prevalence and incidence rates for various faults derived from the 26 studies as well as number of studies quantifying each fault in HVAC system [1]. However, these faults did not include the faults of water pipelines. There is no doubt that the transmission and distribution system occupies a large part of the energy consumption of the air-conditioning system. After being used for a long time, pipes/ducts with or without thermal insulation inevitably suffers damage and leaks. The common faults of hot water pipes in heating mode include pipe blockage, corrosion, leakage and damage and fallen-off of insulation layer. Hallberg et al. indicated that failures on district heating pipes are often caused by water leaks due to corrosion, mechanical impacts and insufficient or deteriorated performance of the thermal insulation solutions [2]. In order to fill the gap in the fault detection and diagnosis of water pipes, we study the three kinds of faults (i. e. pipeline leakage, damaged insulation layer and fallen-off insulation layer) that are often ignored during operation. These faults often do not directly affect the normal operation of the system, but if not repaired in time, they will lead to energy waste and heat loss of the system.

At present, most studies about pipeline fault diagnosis adopt model-based (eg. Ref. [3]), data-driven (eg. Ref. [4]) or the combination of the above two methods (eg. Ref. [5]) to diagnose pipeline leakage [6]. However, these methods are difficult to detect small changes in pressure or flowrate caused by insulation damage or tiny leakage, so it is much difficult to detect and determine the specific location of fault. In addition, these methods rely on sensor data (such as pressure, flowrate, temperature, etc.) collected by building automation systems. However, due to the high cost of the sensor, drift and other faults occur after being used for a long time, the reliability of the data is also reduced. In addition, due to the poor reliability of the control network of the building automation system, problems such as data loss, false positives and confusion of signs are easy to occur. It is obvious that these common fault diagnosis methods cannot address the water pipe problems.

With the maturity of computer vision technology and the existing problems in the fault diagnosis of water pipes in air conditioning system. An automation fault diagnosis method for water pipes based on infrared image is proposed in this paper. The surface temperature of an insulation

* Corresponding author.
E-mail address: xupeng@tongji.edu.cn (P. Xu).

https://doi.org/10.1016/j.buildenv.2022.109111
Received 23 December 2021; Received in revised form 31 March 2022; Accepted 15 April 2022
Available online 26 April 2022

layer is one of the most common indicators that the layer is damaged. For example, the surface temperature distribution of a pipe is abnormal when its thermal insulation layer is damaged. As a nondestructive technique, infrared thermography (IRT) can be employed to remotely measure the temperature of an object and provide the thermal image of an entire component [7]. This technique has been successfully utilized for building diagnostics, such as the evaluation of the thermal performance of building envelopes, electrical inspection, and the detection of air leakages and moisture in building components [8–12]; it is also an effective tool to detect the faults of the thermal insulation layer of pipes.

Recently, a few studies employed IRT for water pipe diagnostics; however, most of them focused on leakage in pipes [13–16]. Ref. [13] developed a novel method utilizing IRT and ground penetrating radar (GPR) technology to detect and locate the leakage point in the pipeline network. GPR is used to find the location of buried pipes, and IRT is for the detection of the leaks. They processed images to isolate the leakage area and calculate its centroid using Green's theorem. Manekiya et al. applied IRT to detect the water leaks of the defected heating pipeline buried in the floor and performed image analysis on the infrared image in MATLAB. They used a threshold-based image segmentation method to obtain the pipeline leakage region and calculate its area [15].

There have been seldom studies relevant to the detection of insulation layer damage in pipes. Fan et al. verified the effectiveness of IRT for detecting defects of the pipeline heat insulation layer, and they analyzed the relationship between the maximum temperature of the infrared thermal image and the size and depth of the heat insulation layer defects [17]. Although they successfully used IRT to inspect the pipelines of a boiler system, methods for detecting faults of the insulation layer were not mentioned in their report. Therefore, their inspection relied on experienced inspectors to collect and judge the infrared images. Wu et al. investigated the changes in soil surface temperature and soil moisture above a buried heating pipeline when it leaked and when its thermal insulation layer was damaged in the laboratory. They concluded that IRT can detect the temperature anomalies caused by leaks and the damaged thermal insulation layer. The humidity difference between the normal and abnormal areas is the key to distinguishing between the two types of failure [18]. However, in their study, there was no clear threshold for the difference in humidity used to distinguish them, and the method has not been tested in practice. In addition, an algorithm based on neural immune ensemble learning is proposed by Xiao Yu to diagnose abnormal high temperature region in infrared steam pipeline image. Later the researcher adopted the same method to diagnose insulation faults [19,20].

The previous studies proved that IRT is an excellent tool to detect abnormal high temperature region, the thermal insulation layer damage and pipe leakage, but there is no denying that other key parameters, such as pressure, are useful for diagnosis. However, no automatic fault diagnosis method and integrated method has been proposed, and these studies can only diagnose one of the failures of pipeline leakage and insulation degradation. Thus, this paper studies three common failures and aimed to develop an automatic algorithm to detect the damage and fallen-off of the thermal insulation layer and leakage of hot water pipes that can be applied in practical buildings by installing infrared cameras in inspection robots or machine rooms. Since the number of additional sensors installed varies depending on the diagnosis method and HVAC system types, it is difficult to judge the initial investment of data-driven diagnosis method against this method. However, it is worth noting that this approach is simple to deploy and easy to maintain. In addition, compared with the previous methods, the method proposed in this paper has the advantages of single data type, non-intrusive monitoring. It can be conducted with inspection robots to diagnose and realize the smart management of air conditioning system.

The rest of this article is organized as follows. In Section 2, the details of the methodology adopted for fault diagnosis are introduced. The performance of the proposed algorithm is evaluated in Section 3 using experimental and actual data. And in Section 4, notes of the algorithm are discussed. Finally, Section 5 concludes the work with a description of the contributions of the study and a discussion of potential work.

2. Methodology

2.1. Overview of the proposed method

As shown in Fig. 1, the proposed algorithm consists of two processes: image segmentation and fault diagnosis. In the first process, to eliminate the influence of the background, gray processing, binarization and mathematical morphological processing are used to isolate the pipe from the background. In the second process, temperature analysis, pipe diameter analysis, and defect analysis are conducted to classify the pipe into three categories: normal, damaged, and fall-off.

2.2. Image segmentation

The main purpose of image segmentation is to eliminate irrelevant information in the image, enhance the detectability of relevant information, so as to improve the reliability of feature extraction, image segmentation, matching and recognition. In this study, Infrared image segmentation is conducted to obtain the infrared image and binary image containing only the pipe area and eliminate the influence of background areas. The flowchart of the image segmentation method used is shown in Fig. 2. Fig. 3 illustrates the processing result of each step of the image segmentation method. The first step of image segmentation is cropping, which can remove the noise of the background in the infrared image, such as the temperature scale and brand logo. The result of cropping is shown in Fig. 3 (b).

2.2.1. Gray processing and threshold processing

Threshold processing is simply and commonly used to separate the object of interest from the background or distinguish objects on the basis of their absolute intensities [21] which can convert a gray image into a binary image. As shown in Fig. 4, pipes in the image are quadrilaterals with uniform width variation, while other heat sources (such as water pump motor, one of the common heat sources in the plant room) are in a certain area of the image. In addition, there is a difference between pipe temperature and the temperature of other heat sources. In the case of normal motor, the pipe temperature and the motor surface temperature are different. Therefore, other heat sources will be removed as background noise as much as possible through threshold processing. Therefore, before threshold processing, gray processing of the raw infrared

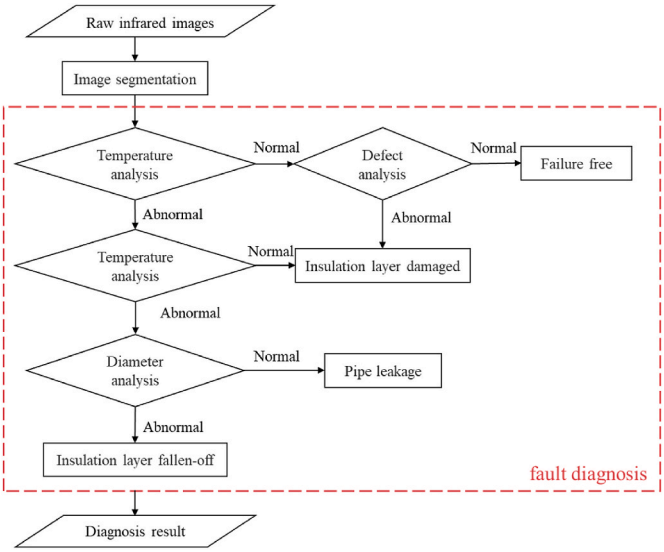

Fig. 1. Framework of the proposed algorithm.

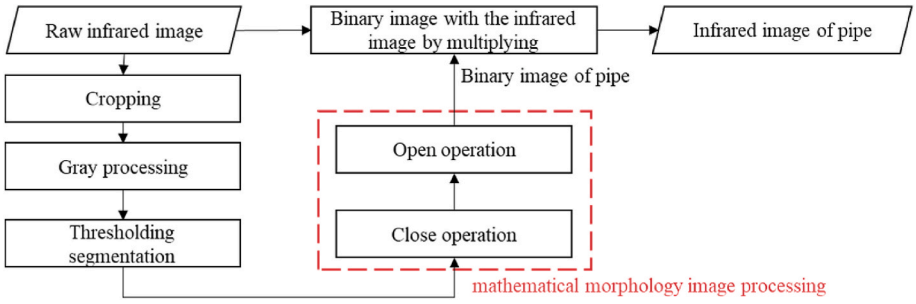

Fig. 2. Flowchart of infrared image segmentation.

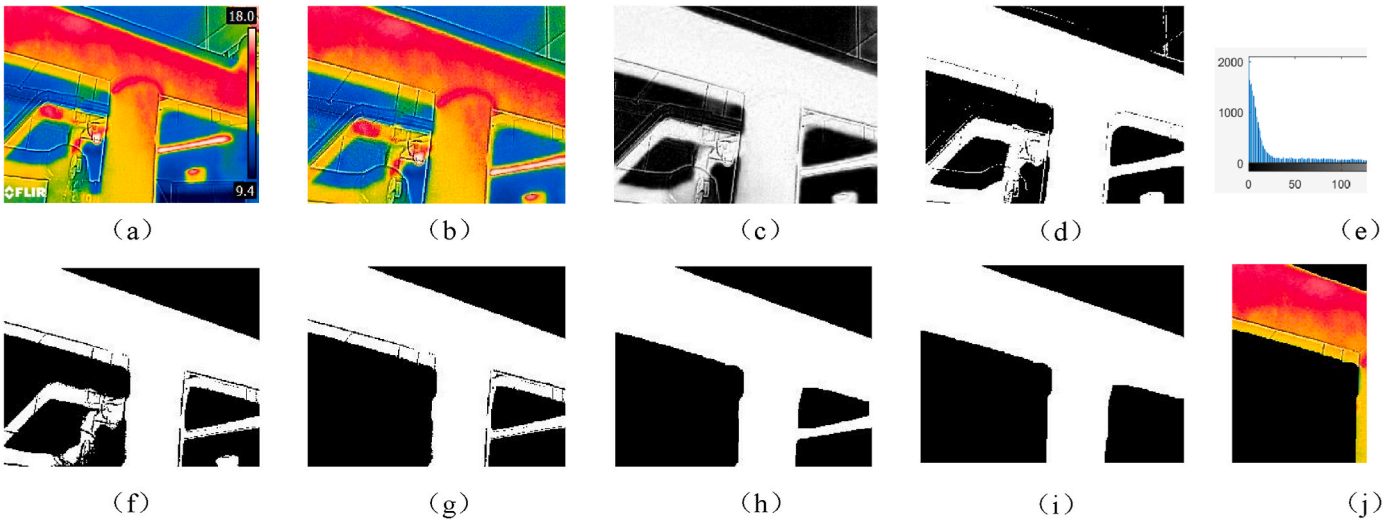

Fig. 3. Image-processing results of image segmentation: (a) raw infrared image, (b) infrared image after cropping, (c) gray image (i.e. the red component image), (d) the segmentation result using Otsu's technique, (e) histogram of the red component image (the red circle indicates the right peak), (f) the segmentation result using the right peak method, (g) the largest connected component of (f), (h) the result of closing, (i) the result of opening (the binary image of the pipe), and (j) the infrared image of the pipe. (For interpretation of the references to color in this figure legend, the reader is referred to the Web version of this article.)

image is necessary because the infrared image is a color image. Considering that the temperature of the hot water pipe is higher than that of the background and the pipe area has a larger red component value in the infrared image, the red component of the raw infrared image (i.e. gray image) is extracted as the input for threshold processing. As Fig. 3 (c) shows, in the red component image, there is a clear difference in gray values between the high-temperature and low-temperature regions.

Thresholding is to select a threshold to divide the grayscale image into background and regions of interest, and it can be expressed as [22]:

$$g(x,y)=\begin{cases}1 & f(x,y)>T\\ 0 & f(x,y)\le T\end{cases} \quad (1)$$

Where $f(x,y)$ is the original grayscale image, and $T$is the set threshold.

Threshold selection has a significant impact on the result of segmentation. Otsu's technique is a commonly used method based on a discriminant analysis, which determines the optimal thresholds by maximizing between-class variance and minimizing within-class variance [23,24]. To separate the pipe and the background more accurately, the gray value corresponding to the right peak of the histogram was selected in this study as the threshold for binarization (as shown in Fig. 3 (e)). As the process results of Fig. 3 shows, compared with Otsu's technique (as shown in Fig. 3 (d)), this method can remove more background regions (as shown in Fig. 3 (f)) and the threshold selected by this method does not vary with variance. However, there are still some small background areas that need to be removed in the binary image after threshold processing. After all connected components in the binary image have been labeled and their area has been calculated, small regions are cleared (as shown in Fig. 3 (g)).

2.2.2. *Mathematical morphology image processing*

Mathematical morphology is a useful tool for smoothing and segmentation [25,26]. Closing can smoothen the contour of an object, connect narrow breaks, and fill holes smaller than the structuring element. Opening also can smoothen the contours; however, as opposed to closing, it can remove regions that are smaller than the structuring element and break thin connections [22]. In this study, a morphological filter consisting of a closing followed by an opening was used. As shown in Fig. 3 (h) and (i), closing fills the small gaps in the pipe area, and opening removes the noise, such as lamps and water pipes of other branches connected to the target pipe in the image. In morphological operation, the selection of structural elements is very important. In this paper, the size of structural element depends on the size of the hole to be filled in closing operation, and the size of the structural element depends on the size of the noise in the infrared image in opening operation. Various experiments have been conducted to determine the appropriate structuring element. In the present case, the structuring elements used in closing and opening are, respectively, 15 × 15 and 20 × 20. Similarly, after the opening operation, the small connected components in the image are cleared.

2.2.3. *Binary image with the infrared image by multiplying*

The result of the above image processing is a pipe binary image without temperature characteristics. By extracting the red, green, and

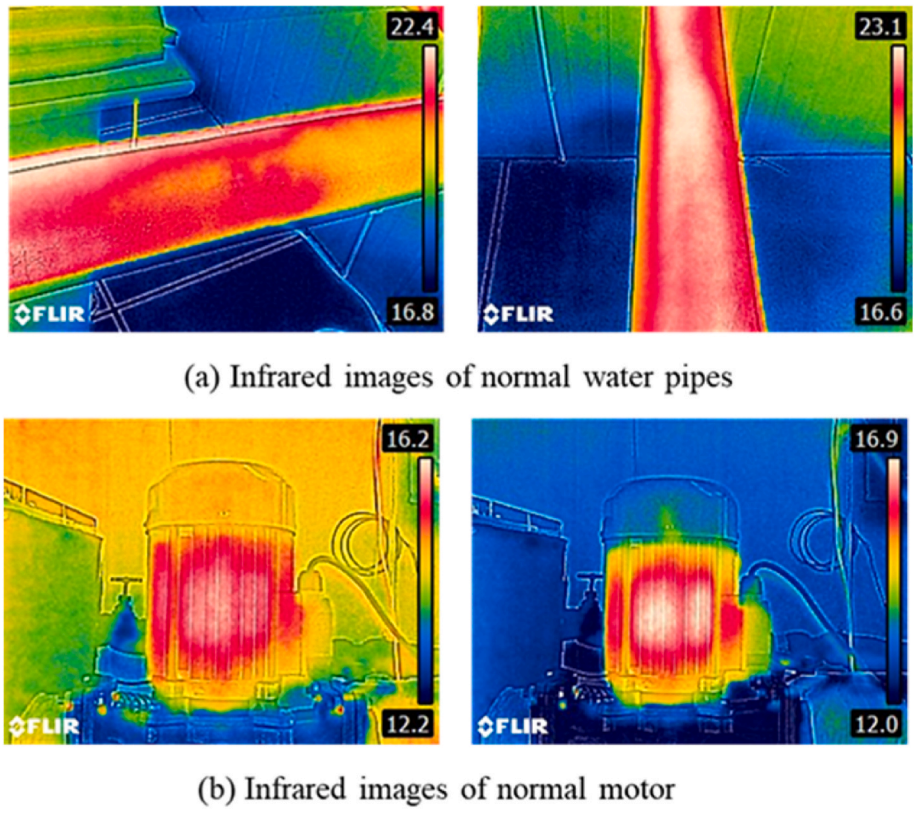

Fig. 4. Infrared images of normal water pipes and normal motor in the plant room.

blue components of the original infrared image, multiplying them by the pipe binary image and then synthesizing them into a color image, one can obtain the pipe infrared image for temperature analysis. As shown in Fig. 3 (j), this method preserves the color of the pipe area in the infrared image and sets the background to black.

2.3. Fault diagnosis

After image processing, three analysis methods including temperature analysis, pipe diameter analysis and defect analysis are conducted to analyze the temperature, pipe diameter and defect characteristics of pipes. Then the fault category can be determined based on the results of feature analysis.

2.3.1. Temperature analysis

The relationship between temperature and color must be established to obtain the temperature information of an infrared image. As shown in Fig. 4, the temperature scale on the right side of the original infrared image was extracted, the upper and lower temperature values were recognized, and linear interpolation was used to obtain the temperature value of each pixel, to determine the relationship between temperature and color based on linear regression. The linear relationship can be expressed as

$$t = \begin{cases} 0 & R = 0, G = 0, B = 0 \\ aR + bG + cB + d & R > 0 \text{ or } G > 0 \text{ or } B > 0 \end{cases} \quad (2)$$

Where t is the temperature, °C; R is the red component value of the pixel; G is the green component value of the pixel; B is the blue component value of the pixel; a, b, and c are coefficients; and d is a constant. They are all decided by linear regression.

As mentioned above, the background of the infrared image is black, and its temperature value is set to zero in this part. The processed image is an infrared image, so there are only two parameters in the linear model, namely a and d. After determining the linear relationship between temperature and color, the temperature matrix of the entire image can be obtained. The point where the temperature value is zero corresponds to the background and is eliminated when performing temperature analysis.

An optical character recognition (OCR) system typically consists of several phases, including extraction, localization, segmentation, and recognition [27]. The FLIR-E6 camera used in this study can automatically identifies cold or hot spots until temperature limits are captured when taking infrared images. Other specific technical parameters are listed in Table 1. First, because the locations of the temperature scales are fixed (the location of the temperature scales is on the right of the image taken by FLIR-E6 camera as shown in Fig. 9) and the upper and lower limits of temperature are respectively at the upper and lower parts of the temperature scale if the images are taken by the same device, cropping was used to extract the upper and lower temperature limits from temperature scales which are equally important to the later linear model. Second, to locate the characters, the parts of the image that did not contain characters were eliminated after thresholding based on Otsu's technique. The segmentation was then realized vertically to divide the characters. The division used a histogram to look for columns that do not have any white pixel, which is considered as a region to cut [28]. The sample of segmentation results can be seen in Fig. 5. Finally, in character recognition, a template matching technique was used to recognize the characters, and all the templates were extracted from the

Table 1
FLIR-E6 camera specification.

IR resolution	160 × 120
Thermal sensitivity	<0.06 °C
Spatial resolution (IFOV)	5.2 mrad
Object temperature range	−20–250 °C
Accuracy	±2 °C or ±2% of reading

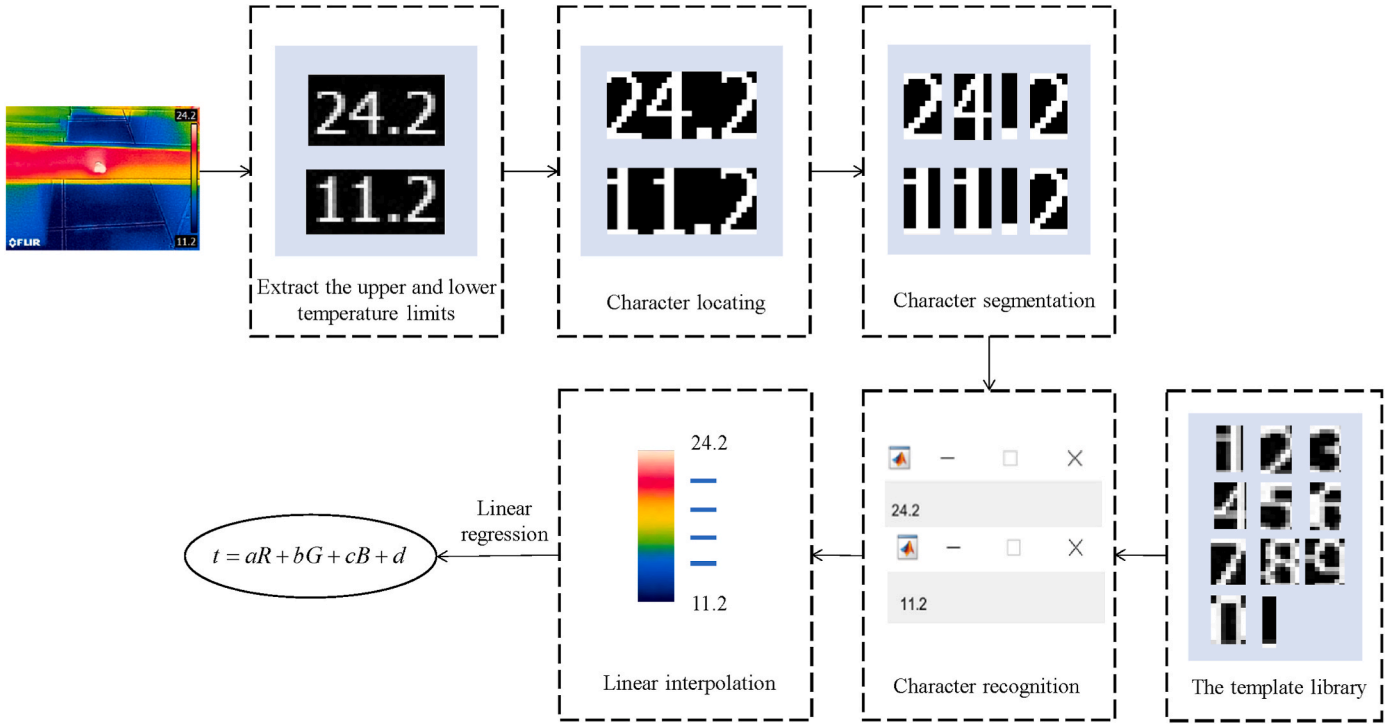

Fig. 5. Temperature–color linear relationship establishment process. (For interpretation of the references to color in this figure legend, the reader is referred to the Web version of this article.)

captured infrared images by the abovementioned extraction, localization, and segmentation. Based on the characteristics of pixel distribution, the character to be recognized was adjusted to the same size as the templates, compared with the templates, and classified into the category of the template with the maximum number of identical pixels. The recognition result of the rightmost character is the number after the decimal point, that of the second character on the right is the decimal point, that of the third character on the right is the ones digit, and that of the fourth character on the right is the tens digit (if there is no fourth character on the right, its recognition result is set to 0). Although there is a powerful OCR tool in MATLAB, this method performed better in this case.

After identifying the values of the upper and lower temperature limits, the temperature scale image was extracted, a column of 181 pixels was taken for linear interpolation, and the result of linear interpolation was used as training data to obtain the linear relationship between temperature and color. In addition, the upper and lower temperature values varied from one image to another; thus, the relationship between temperature and color needed to be obtained for each infrared image.

The 3σ rule is a common criterion for discriminating significantly abnormal data in data cleaning, which is based on normal distribution, and the data outside the interval (μ-3σ, μ+3σ) is considered abnormal data. If there is no fault in the pipe, the external surface temperature of the pipe in the image should follow the normal distribution. Therefore, this paper adopts 3σ to judge whether there are significantly abnormal temperature values in the water pipe area. Following getting the average temperature of the pipe $\bar{t}$and the standard deviation of the temperatures, the 3σ rule was adopted to determine whether there were abnormal temperatures in the pipe area. In particular, the average value of the first 1% maximum temperature was taken as the maximum temperature of the water pipe area tm to determine whether it was higher than $\bar{t} + 3\sigma$. If it was higher, this water pipe was considered to be a faulty water pipe; otherwise, the water pipe was considered not faulty. In addition, we also adopted temperature analysis methods when identifying leaking pipes and pipes with falling off the insulation layer. Because the temperature of the air-conditioning hot water and the temperature of pipe where the insulation layer falls off are much higher than the surface temperature of the pipe with insulation layer, we stipulate that the pipe leaks or the insulation layer falls off when tm-$\bar{t}$>4 °C, and the constant is determined through several tests.

2.3.2. Pipe diameter analysis

The purpose of pipe diameter analysis is to identify pipes where the insulation layer has fallen off. As shown in Fig. 6 (a), if the thermal insulation layer of the hot water pipe falls off, the diameter of that section of the pipe is smaller than that in the other sections. In this study, the diameter of a horizontal pipe was defined as the sum of the pixel values in each column. To analyze the diameter characteristics of a pipe lacking a part of the insulation layer, Fig. 6 illustrates the binary images and the pipe diameter difference curves of three horizontal pipes: a pipe with a part of the insulation layer fallen off, a normal pipe, and a normal T-shaped pipe. The pipe diameter difference graph depicts the relationship between the columns and the diameter difference between the current column and the subsequent 60th column. As Fig. 6 (b) shows, the pipe diameter difference of the normal pipe was small, with a maximum of three pixels. However, for the other two pipes, the pipe diameter difference varied significantly with the columns. Moreover, in contrast to the pipe with a part of the insulation layer fallen off, the pipe diameter of the T-shaped pipe increased at a certain section; therefore, the column corresponding to the maximum diameter difference was greater than the column corresponding to the minimum.

Hence, the method for pipe diameter analysis is as follows.

Step 1	Obtain the maximum and minimum row values of the pipe area and calculate the height of the water pipe area. If the height of the water pipe area is equal to the image height, the pipe is vertical, and the image needs to be rotated 90° counterclockwise.
Step 2	Count the number of pixels with a pixel value of 1 in each column as the pipe diameter.
Step 3	Starting from the first column, calculate the diameter difference between the column$j$and the column$j + p$.

(*continued on next page*)

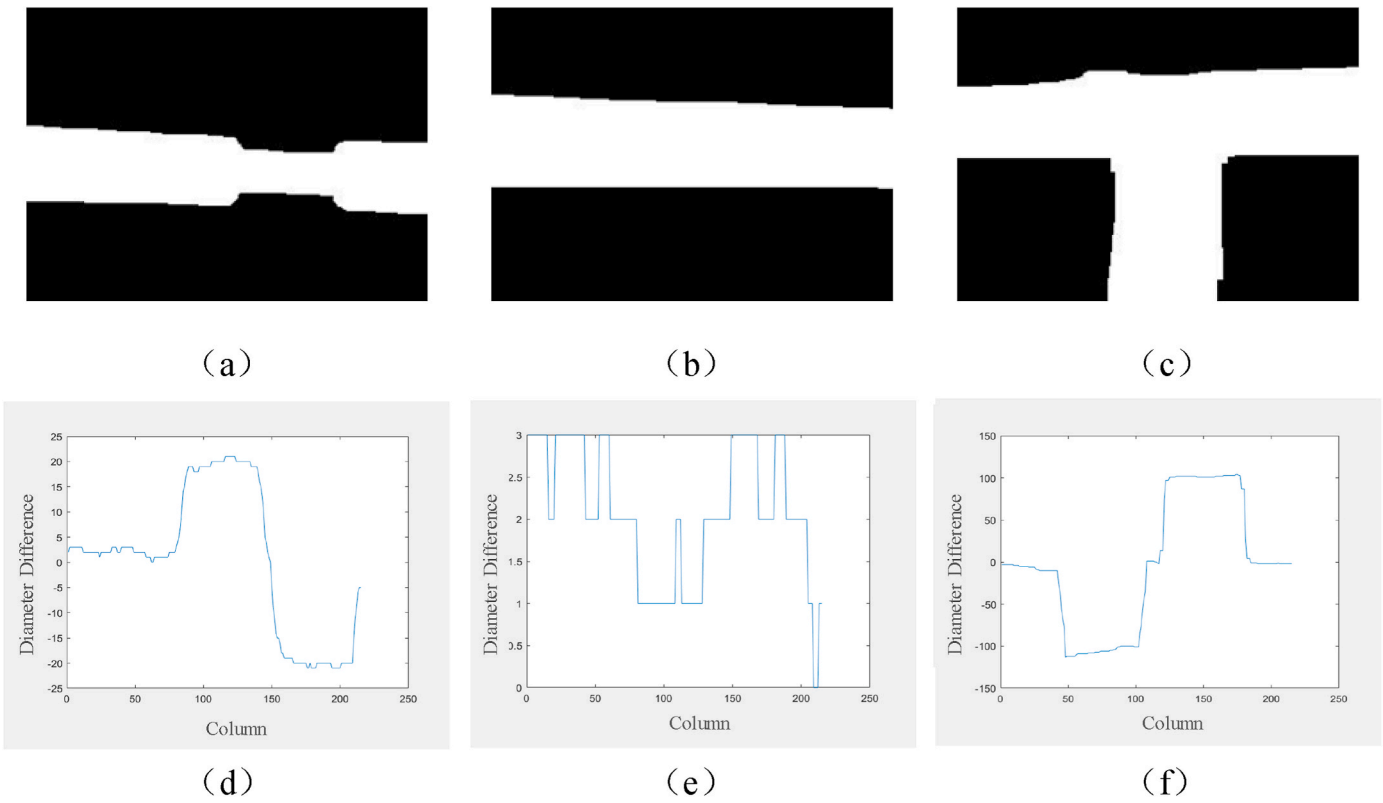

Fig. 6. Pipe diameter characteristics of different pipes: (a) the binary image of a pipe with a part of the insulation layer fallen off, (b) the binary image of a normal pipe, (c) the binary image of a normal T-shaped pipe, (d) the pipe diameter difference curve of (a), (e) the pipe diameter difference curve of (b), and (f) the pipe diameter difference curve of (c).

(*continued*)

Step 4	Obtain the maximum diameter difference D_m and its column m. Obtain the minimum diameter difference D_n and its column n.
Step 5	When $D_m > k$, $m < n$, and $\|\|Dm\| - \|Dn\|\| < a$, the part of the thermal insulation layer is missing; otherwise, the insulation layer does not fall off.

The values of p, k, and a are related to the thickness of the thermal insulation layer and the size of the binary image. In this case, p is 60, k is 16, and a is 10.

2.3.3. Defect analysis

When the damage depth of the pipe insulation layer is shallow, the temperature analysis may not be sufficient to detect the fault. Therefore, in this study, defect analysis was conducted to determine whether there was an abnormal high-temperature damage zone in the pipe area.

Edge detection methods have been widely used to detect defects of pipes and ducts, and they have performed well [29,30]. In the defect analysis, the edge detection method was used to extract the edges of the internal defects of the water pipe and fill it to examine whether its area was greater than 0 and its maximum temperature was close to the maximum temperature of the water pipe area. The specific steps are shown below.

Step 1	The Canny algorithm [31] is used for the binary image of the water pipe to extract the outer edge of the water pipe, and the dilation of the edge by a 20 × 20 structuring element is recorded as H.
Step 2	Obtain the blue component I_s of the infrared image of the pipe, and use the Canny method to extract edges I.
Step 3	Calculate $K = I - H$, and $K$is the inner edge of the pipe.
Step 4	Calculate $J = I_s \times K$, processing J by Otsu's method and connecting fracture edges.
Step 5	Fill holes formed by closed edges and subtract $K$to obtain the filled area.

(*continued on next column*)

(*continued*)

Step 6	Calculate the area of the filled area S and its maximum temperature t_s. If $S > 0$ and $t_m - t_s < 0.1$, the insulation layer is damaged; otherwise, the insulation layer is not damaged.

Fig. 7 shows the image-processing results of defect analysis. Fig. 7 (a) and (b) are the binary image and infrared image of the pipe respectively First, the Canny algorithm was used to extract the edges of the binary image of the pipe and thicken the outer edges of the water pipe by dilation, as shown in Fig. 7 (c) and (d).

Similar to the previous binarization processing, when extracting the overall edge information of the pipe, the blue component of the pipe infrared image was selected for processing, because the defect area appeared approximately white in the infrared image, having larger blue component values than other areas of the pipe. As shown in Fig. 7(e), there were obvious differences in gray values between the defective part and other areas.

By obtaining the edges of the blue component image based on the Canny method and subtracting the outer edges, one can obtain the inner edges of the pipe, as shown in Fig. 7(g). To remove more noise and eliminate the edges of non-defective areas, a multiplication operation was performed with the blue component image and the internal edge image, and then the image binarization was conducted, as shown in Fig. 7(i).

Unfortunately, the edges are not continuously connected. Therefore, an edge connection algorithm was used to connect the edges, identifying and connecting the endpoints that meet the distance requirements [32]. Finally, the closed edges were filled and the edges were subtracted to obtain the binary image of the filled area, as in Fig. 7(l).

In the defect analysis, the index to determine whether there was a defect in the insulation layer was the area and maximum temperature of the filled area, where the area was the total number of pixels with a pixel

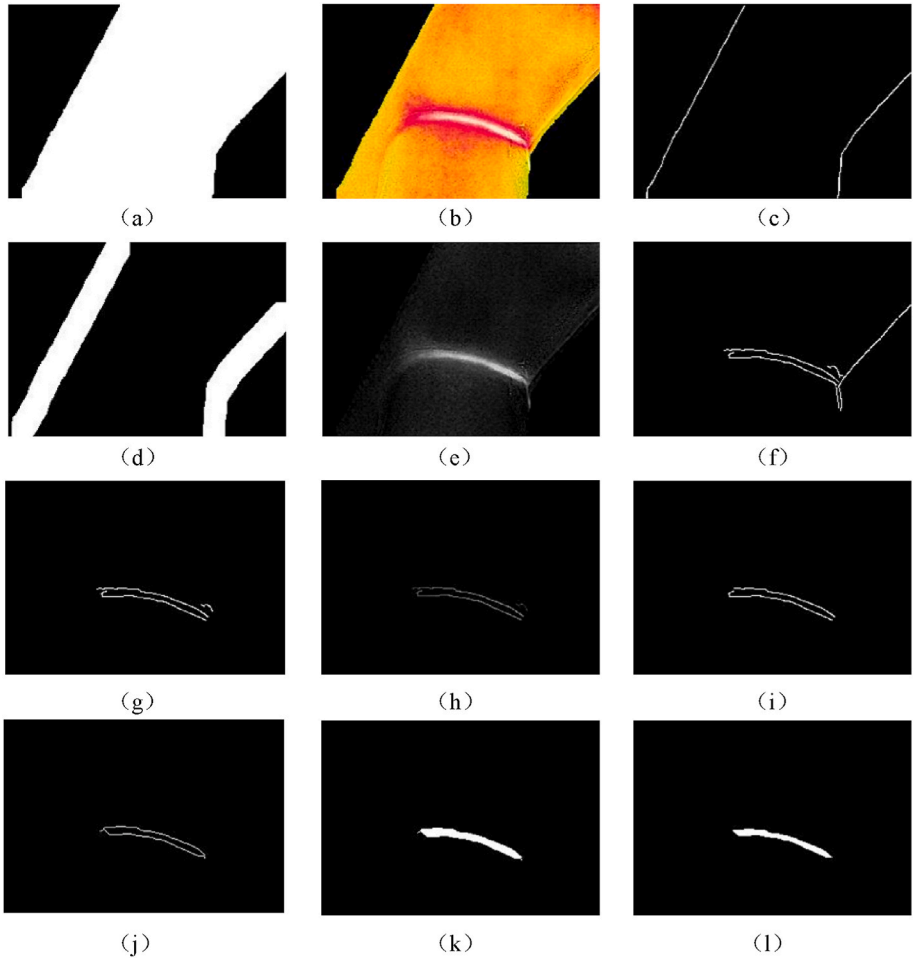

Fig. 7. Image-processing results of defect analysis: (a) binary image of the pipe, (b) infrared image of the pipe, (c) outer edge of water pipe, (d) dilation of (c), (e) blue component of (b), (f) edges extracted from (e), (g) the inner edge of the water pipe, (h) the edge in the blue component image, (i) the binary image of (h), (j) the edge connection result, (k) the filling result, and (l) the filled area. (For interpretation of the references to color in this figure legend, the reader is referred to the Web version of this article.)

value of 1, and the maximum temperature was the average of the first 1% maximum temperature. If the area was greater than 0 and the maximum temperature was close to the maximum temperature of the water pipe area, the insulation layer was damaged; otherwise, the insulation layer was considered sound.

In the defect analysis, the parameters were the results of various experiments, which were determined according to the actual situation, such as image size, pipe size, and defect size. In addition to the structuring element used for dilation, in this study, the upper and lower thresholds of the Canny algorithm were, respectively, 0.3 and 0.16, and the distance set in the edge connection was 5 pixels.

2.3.4. Flow of fault diagnosis

Based on the above three analyses, a fault diagnosis process was formulated, as shown in Fig. 8. The first step was to carry out a temperature analysis to determine whether the pipe temperature was abnormal; if it was, it is further determined whether the temperature difference between the highest temperature and the average temperature is greater than 4 °C. When it is not greater than 4 °C, it is considered that the water pipe maybe have an insulation damage failure; otherwise, diameter analysis is conducted. When the diameter characteristics of the pipe were consistent with those of the pipe with a part of the insulation layer removed, the insulation layer was determined to be; otherwise, the pipe was classified as leakage. For cases where the pipe temperature was normal, if the defect analysis showed there was no high-temperature damaged area in the infrared image, the pipe was considered normal; otherwise, if further temperature analysis indicates the temperature difference between the highest temperature and the average temperature is not greater than 4 °C, its insulation layer was considered damaged.

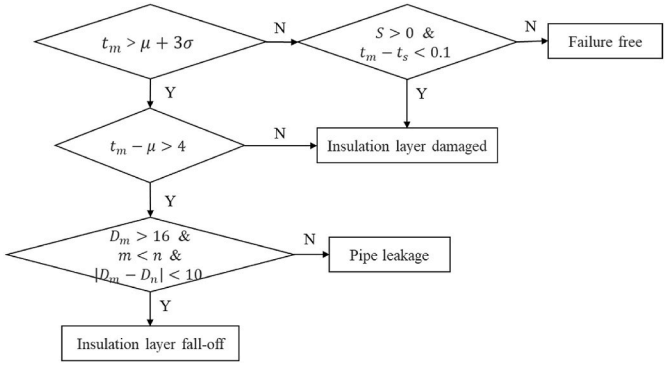

Fig. 8. Flowchart of fault diagnostic.

3. Results and analysis

3.1. Evaluation indicators

In this study, the classification performance was measured based on the confusion matrix, which displays the classification results in rows and the actual values in columns. The percentage of accuracy (ACC), precision (P), recall (R), and *F*1 were selected as indicators to evaluate the performance of the proposed algorithm for the experimental and actual data. The relevant definitions are as follows [33].

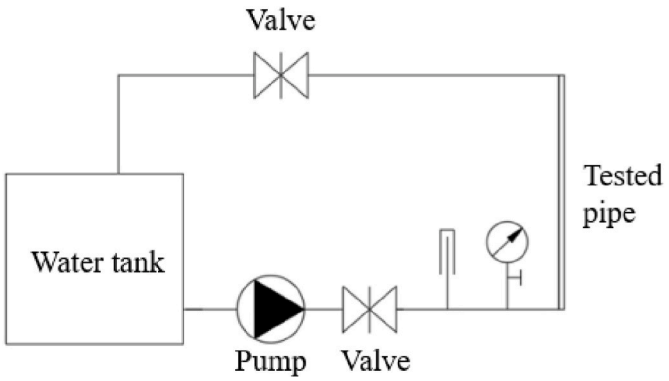

Fig. 9. Flowchart of fault diagnostic.

$$ACC = \frac{n_{TP} + n_{TN}}{n_{TP} + n_{TN} + n_{FP} + n_{FN}}$$

$$P = \frac{n_{TP}}{n_{TP} + n_{FP}}$$

$$R = \frac{n_{TP}}{n_{TP} + n_{FN}}$$

$$F1 = \frac{2 \times P \times R}{P + R}$$

Where n_{TP} is the number of positive samples classified correctly, n_{TN} is the number of negative samples classified correctly, n_{FP} is the number of positive samples classified incorrectly, and n_{FN} is the number of negative samples classified incorrectly.

3.2. Experimental results

3.2.1. Test setup and experimental procedure

To obtain infrared images of normal and faulty hot water pipes, an experimental platform was set up, consisting of a water tank, a water pump, two valves, a thermometer, a pressure gauge, and pipelines, as shown in Fig. 9. The size of the water tank was 500 × 500 × 300 mm (length × width × height), and the diameter of the galvanized steel pipes was 40 mm. Rubber foam was used as the thermal insulation material for the heat preservation of the water tank and pipeline. The right pipe was the tested pipe, whose two ends were screw-threaded connections, which was convenient for disassembly to replace different types of pipes. The experimental steps were as follows.

a. Prepare a normal or faulty pipe as the tested pipe and connect it to the system.
b. Fill the water in the water tank to the standard water level and heat it to 50–60 °C with an electric heater.
c. Turn on the water pump and start the system. After the system is stable, acquire the infrared images of the tested pipe.

3.2.2. Experimental results

A total of 290 infrared images with a size of 320 × 240 were obtained from the experiments: 64 images of healthy water pipes, 101 images of pipes with a damaged thermal insulation layer, 43 images of pipes with a part of the thermal insulation layer fallen off and 82 images of pipes with leakage. The typical images of the four types of pipes are shown in Fig. 10, demonstrating that the temperature distribution of the fault-free water pipe was uniform. The infrared image of the faulty water pipe has obvious temperature anomalies.

Table 2 summarizes the confusion matrix of the test results of the algorithm applied to experimental data, whose diagonal is the number of samples diagnosed correctly. The rest are the number of samples diagnosed incorrectly. The table shows that three images of normal pipes were classified as pipes with damaged insulation layers, three images of pipes with damaged insulation layers that were diagnosed as normal pipes, and one image of a pipe with a part of thermal insulation layer fallen off was diagnosed as leakage. Most of the misclassification occurs between normal pipes and pipes with damaged insulation layer. As can be seen from Fig. 11 (a), the insulation layer of the pipeline is slightly depressed (we consider the pipe is normal). And in Fig. 11 (b), although the insulation layer damage occurred in this pipe, it was wrongly classified as normal pipe due to the small scope of damage. After comparison, it was found that the infrared image of slight sag and slight damage of insulation layer is very similar, so it will cause misclassification between them. No other reason of misclassification was found. Fig. 11 (c) and (d) respectively show the infrared image of the fallen-off insulation layer misclassified as leakage and an infrared image of pipeline leakage. From the perspective of temperature distribution, one side of the temperature distribution in both images has abnormally high temperature. From the perspective of pipe diameter, there is a phenomenon of pipe diameter reduction. That is to say, when insulation falls off at the pipe joint or pipe diameter reduction, it may be misclassified as leakage. Therefore, only 7 of the 290 images were diagnosed incorrectly, and the proportion of correctly classified samples accounted for 97.59% of the total samples, indicating that the algorithm has a high accuracy.

Table 3 lists the performance indicators of the algorithm based on the

Table 2
Confusion matrix obtained from the evaluation of the algorithm using experimental data.

Estimated	Actual			
	Normal	Damaged	Fallen off	Leakage
Normal	61	3	0	0
Damaged	3	98	0	0
Fall-off	0	0	42	0
Leakage	0	0	1	82

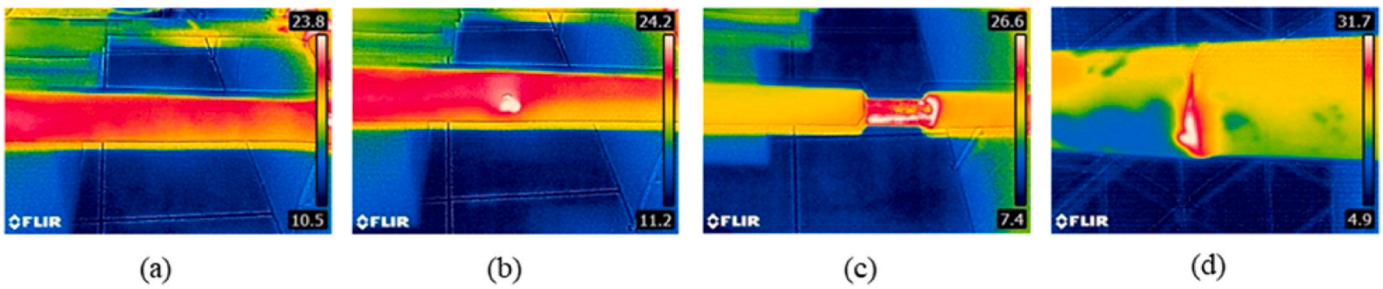

Fig. 10. Infrared images captured from the experiments: (a) infrared image of a healthy pipe, (b) infrared image of a pipe with a damaged thermal insulation layer, (c) infrared image of a pipe with a part of the thermal insulation layer fallen off, and (d) infrared image of a pipe with leakage.

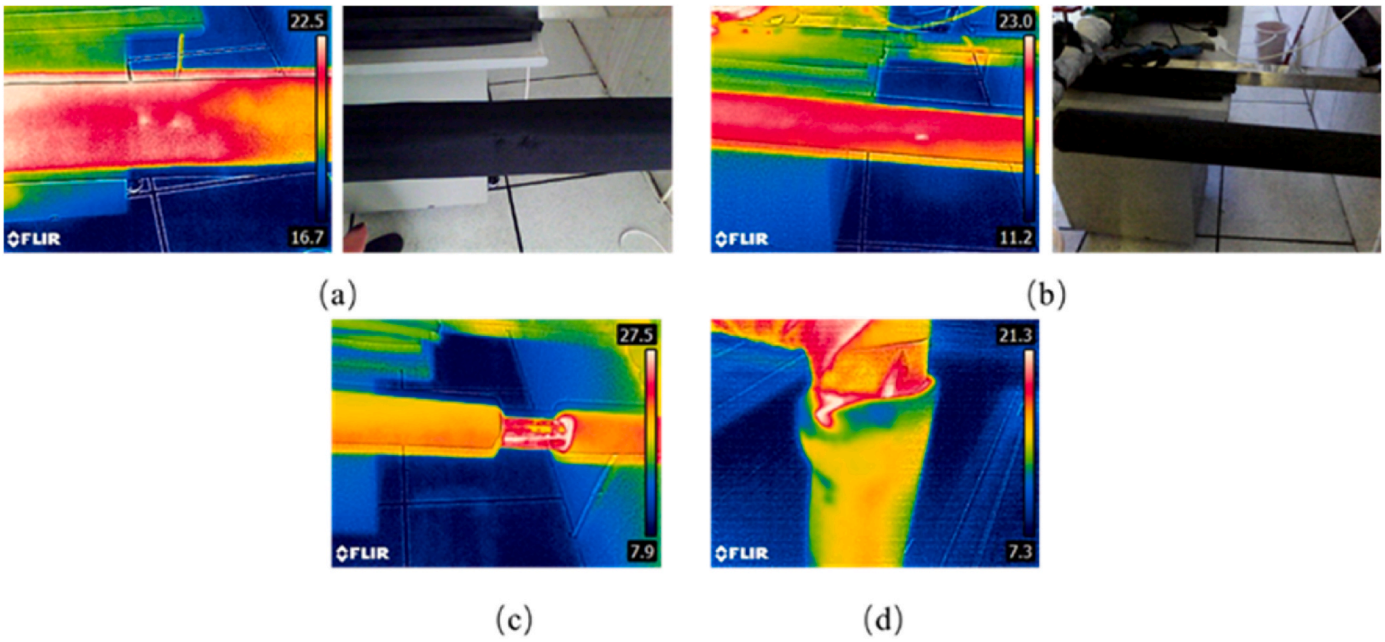

Fig. 11. Images of misclassified pipes: (a) images of a normal pipe that is misclassified into a pipe with a damaged thermal insulation layer, (b) images of a pipe with a damaged thermal insulation layer that is misclassified into a normal pipe, (c) the infrared image of the fallen-off insulation layer misclassified as leakage, (d) an infrared image of pipeline leakage.

Table 3
Performance indicators of the algorithm evaluation using experimental data.

Class	Accuracy (%)	Precision (%)	Recall (%)	F1 (%)
Normal	97.93	95.31	95.31	95.31
Damaged	97.93	97.03	97.03	97.03
Fall-off	99.65	97.67	100.00	98.82
Leakage	99.66	100.00	98.80	99.40
Average	98.79	97.50	97.79	97.64

above-mentioned confusion matrix, including classification accuracy, precision, sensitivity, and specificity for normal, damaged, fall-off classes. The classification accuracies of the classifier for normal, damaged, and fallen off, and leakage were, respectively, 97.93%, 97.93%, 99.65% and 99.66%. The average per-class accuracy, precision, recall, and *F*1 were 98.79%, 97.50%, 97.79%, and 97.64%, respectively. In practical applications, because of the waste of labor and time, people are often worried that the normal pipes will be recognized as faulty pipes. The accuracy rate of normal water pipes in Table 3 indicates that the probability of such misjudgment is 2.07%. Therefore, under the experimental conditions, the algorithm can accurately detect and isolate insulation faults of water pipes with good performance.

3.3. Case study

In order to know if this method can be applied in practice, a typical commercial building is selected for testing. In this study, images of hot water pipes in the heating, ventilation, and air conditioning (HVAC) plant room in this commercial building plant room were collected as actual data to evaluate the performance of the developed algorithm. Since it is difficult to collect images for the other two types of failure and the time to capture images is limited, the infrared images and visual images of a normal pipes and pipes with an obviously damaged insulation layer collected in the plant room, as shown in Fig. 12. The plant room had been used for a long time, and the thermal insulation layer was damaged. The temperature of the damaged zone in the infrared image was significantly higher than the temperature of the normal area of the water pipe, making it more easily recognized than in the visual image. Therefore, it is more reliable to use the infrared thermal-imaging technique for fault detection than the naked eye. In the field investigation of the air-conditioning water system, the damage of the insulation layer mostly occurred at the joints of pipelines, which relevant personnel or machines should pay more attention to when performing an inspection.

Because there were no pipes with a part of thermal insulation layer fallen off and leakage in the plant room of the New Jiangwan Cultural Center, only the images of two types of pipes were collected. The actual data consisted of 124 infrared images: 27 images of normal water pipes and 97 images of pipes with a damaged thermal insulation layer.

Table 4 summarizes the confusion matrix as the test results of the algorithm on actual data. Table 5 lists the performance indicators of the algorithm based on the abovementioned confusion matrix, including classification accuracy, precision, sensitivity, and specificity for normal and damaged classes. For the actual data, 115 of the 124 images were classified correctly, accounting for 92.74% of the total samples. Compared with the experimental results, the diagnostic accuracy of the algorithm in the actual building was relatively low, because the actual infrared image was more complicated than the experimental infrared image. As shown in Fig. 12 (c), the noise of the infrared images taken in practical buildings includes not only the surrounding pipes but also the lamps in the plant room. Because of this, the images of normal pipes in practical buildings are often misjudged as faulty pipes. Therefore, when collecting images, a suitable angle for taking pictures should be chosen to avoid the effects of surrounding pipes and lights. Furthermore, appropriate structuring elements should be used for the opening operation in image segmentation to remove the most noise.

4. Discussion

The method can be used with the infrared camera installed on the intelligent inspection robot. It has a high accuracy in the diagnosis process of experimental and actual buildings, but there are some notes about the application of this algorithm:

1) The size of structural element depends on the size of the hole to be filled in closing operation, and the size of the structural element depends on the size of the noise in the infrared image in opening

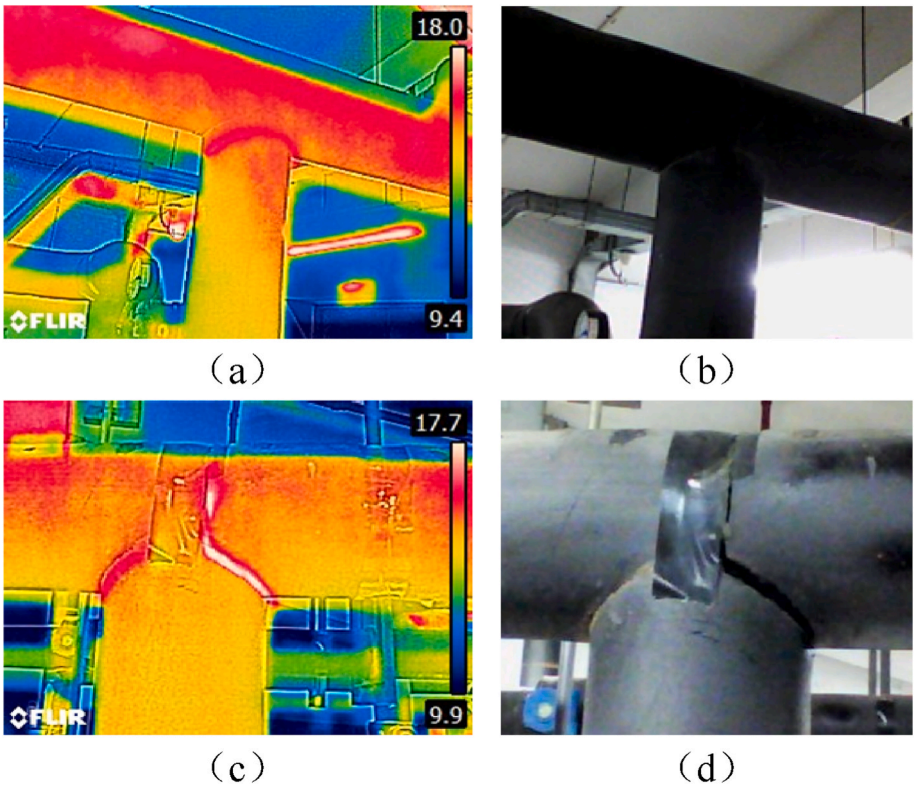

Fig. 12. Images captured in actual buildings: (a) the infrared image of a normal pipe, (b) the visual image of (a), (c) the infrared image of a pipe with a damaged insulation layer, and (d) the visual image of (c).

Table 4
Confusion matrix obtained from the evaluation of the algorithm on actual data.

Estimated	Actual	
	Normal	Damaged
Normal	23	5
Damaged	4	92

Table 5
Performance indicators of the algorithm evaluation on experimental data.

Class	Accuracy (%)	Precision (%)	Recall (%)	F1 (%)
Normal	92.74	85.19	82.14	83.64
Damaged	92.74	94.85	95.83	95.34
Average	92.74	90.02	88.99	89.49

operation. If the size of the infrared image changes, adjusting the relevant parameters for image processing in image segmentation, pipe diameter analysis, and defect analysis is recommended.

2) The algorithm has certain requirements for the image, or it might lead to misclassification. It is necessary to ensure that the hot water pipe is a high-temperature region in the infrared image and to minimize hotpots other than the water pipe, such as lamps, other water pipes or other heat sources. Therefore, when collecting image data, a suitable angle should be selected to avoid the influence of surrounding pipes and lighting in the machine room as much as possible.
3) If the infrared camera is installed on the inspection robot, it should be taken into account when planning the inspection route to ensure 360° full picture of the water pipe. In addition, the damage of the water pipe insulation layer mostly occurs at the joints of the water pipes, where the inspectors should take more photographs when performing regular inspection and maintenance. In our previous study, intelligent inspection robot has been put into use to fulfil the inspection task of the machine room. The composition of the robot is shown in Fig. 13. It can carry out all-day and high-frequency inspection according to the specified path and the task positions (Fig. 14 gives an example of the inspection route and task positions of the inspection robot in a plant room). The reliable data obtained by inspection robot can combine with the fault diagnosis algorithm to ensure the normal operation of the plant room.
4) As for other faults, for example, pipe blockage, although it is not within the scope of this paper, temperature abnormality can also be detected in the temperature analysis. Even if it is misclassified as leakage or damaged or fallen-off insulation, an alarm can be issued to remind timely repair of the fault.

5. Conclusion

An automatic diagnosis algorithm based on infrared images was proposed to detect pipeline failures are often ignored (i.e. damaged insulation layer, the fallen-off thermal insulation layer and leakage) using infrared thermal images including abnormal information. Compared to previous methods, the new method has three advantages. Firstly, the previous method (i.e. pressure-based approach) cannot detect the small changes caused by insulation damage or tiny leakage. That is to say, the previous method cannot detect the insulation damage or tiny leakage. Secondly, the method in this paper will not be affect by drift and other faults of sensors. Moreover, this method is easy to deploy and to maintain. Another advantage is non-invasive when collecting images, so it is available in existed building and don't affect the operation of system. The diagnosis algorithm includes image segmentation and fault diagnosis. Gray processing, binarization and mathematical morphological methods were adopted in image segmentation to extract the pipe area in the infrared image. Since the infrared images of these are similar, three analyses are adopted to identify the differences and develop classification rules. Temperature analysis is conducted to

Fig. 13. Components of intelligent inspection robot.

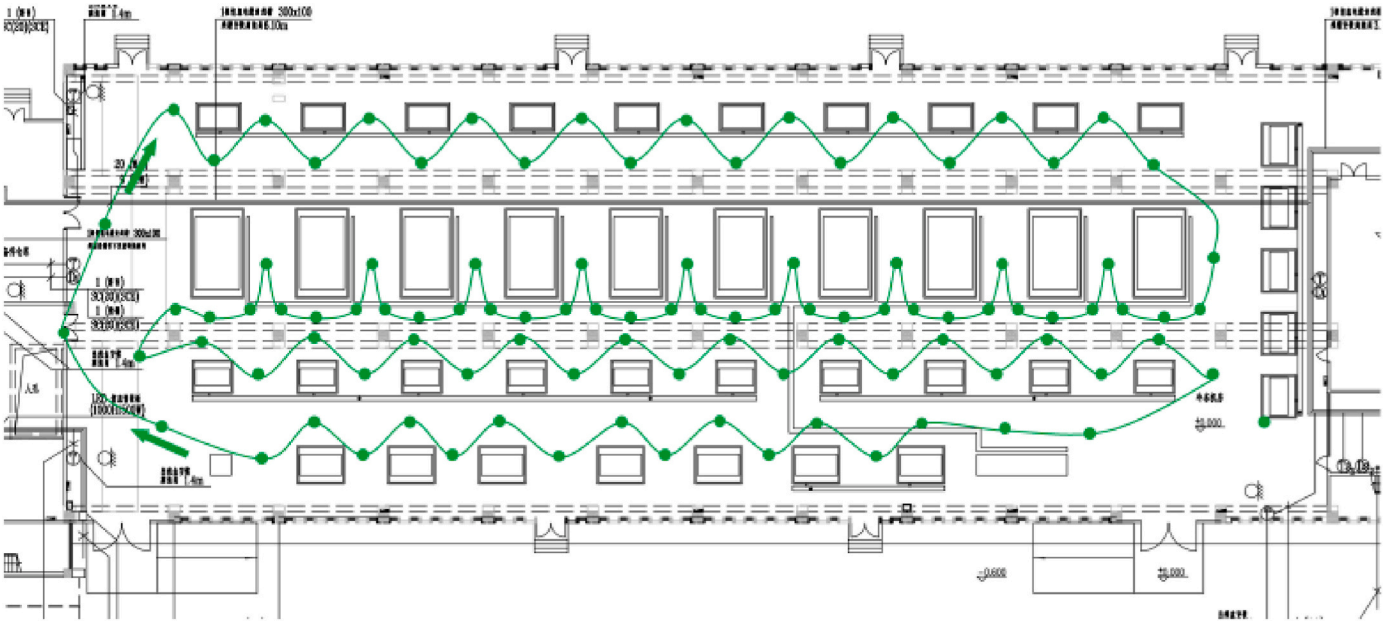

Fig. 14. The specific route and part of task positions of the inspection robot (In fact, there are more task points than are shown in the figure).

examine whether the temperature of the pipe is abnormal. Pipe diameter analysis is applied to determine whether the thermal insulation layer has fallen off. Defect analysis is used to detect the defects inside the pipe area. In order to evaluate performance of the diagnosis method, accuracy, precision, recall and F1 score are adopted to evaluate the diagnosis algorithm. The conclusion are as follows:

1) First of all, we set up the experimental platform, and collected the infrared and visible images of these faults for all types of faults. The results show the accuracy of the algorithm was 97%.
2) In order to test whether the algorithm can be applied in practice, a typical commercial building is selected for testing. Due to time constraints, we only collected infrared images of normal pipes and pipes with damaged insulation layer, and the accuracy of the algorithm is 93%. It can be said that the algorithm can be applied in actual buildings.
3) On the whole, the algorithm was relatively robust, and it can be said that the algorithm was relatively robust. And due to the advantages of single data type, non-intrusive monitoring and convenient deployment compared the data-based method, it can be applied in an infrared camera installed on an inspection robot or in a machine room.

6. Limitation and future work

Although the proposed algorithm can accurately identify three faults of water pipes in an HVAC system, the severity of the fault has not been evaluated, and further research on this is needed. Moreover, this method cannot distinguish the insulation layer falling off at the pipe joint and the reduction in pipe diameter. However, due to the low probability of such misclassification, we ignore this shortcoming in our study. This will be considered in future studies. It should be noticed that this study only studies three common failures, some other faults using infrared images collected by non-invasive devices, such as pipe blockage, cannot be identified. More data (such as the changes of pressure or flowrate collecting by invasive sensors) are needed to assist the method to diagnose pipe blockage or other faults. Due to the viscosity of the fluid, temperature, pipe size, there will be a pressure drop between the two positions of pipe system. If there is no fault, the pressure drop should be normal. While fault occurs, such as pipe blockage, the pressure drop will be abnormally high. The combination of non-invasive and invasive method for fault diagnosis is our future work. In addition, more tests in actual building are needed to verify the reliability of the proposed method.

CRediT authorship contribution statement

Hang Guan: Conceptualization, Methodology, Validation, Writing – original draft. **Tong Xiao:** Writing – review & editing, Data curation. **Wei Luo:** Visualization, Writing – review & editing. **Jiefan Gu:** Writing – review & editing. **Ruikai He:** Writing – review & editing. **Peng Xu:** Writing – review & editing, Supervision.

Declaration of competing interest

The authors declare that they have no known competing financial interests or personal relationships that could have appeared to influence the work reported in this paper.

References

[1] Janghyun Kim, Kim Trenbath, Jessica Granderson, et al., Research challenges and directions in HVAC fault prevalence, Sci. Technol. Built Environ. 27 (5) (2021) 624–640, https://doi.org/10.1080/23744731.2021.1898243.

[2] D. Hallberg, B. Stojanović, J. Akander, Status, needs and possibilities for service life prediction and estimation of district heating distribution networks, Struct. Infrastruct. Eng. 8 (1) (2012) 41–54, https://doi.org/10.1080/15732470903213740.

[3] C. Liu, Y. Li, M. Xu, An integrated detection and location model for leakages in liquid pipelines, J. Petrol. Sci. Eng. 175 (2019) 852–867, https://doi.org/10.1016/j.petrol.2018.12.078.

[4] P. Xue, et al., Machine learning-based leakage fault detection for district heating networks, Energy Build. 223 (2020), https://doi.org/10.1016/j.enbuild.2020.110161.

[5] D. Zaman, et al., A review of leakage detection strategies for pressurised pipeline in steady-state, Eng. Fail. Anal. 109 (2020), https://doi.org/10.1016/j.engfailanal.2019.104264.

[6] S. Buffa, et al., Advanced control and fault detection strategies for district heating and cooling systems-A review, Appl. Sci. 11 (1) (2021), https://doi.org/10.3390/app11010455.

[7] S. Bagavathiappan, et al., Infrared thermography for condition monitoring - a review, Infrared Phys. Technol. 60 (2013) 35–55, https://doi.org/10.1016/j.infrared.2013.03.006.

[8] C.A. Balaras, A.A. Argiriou, Infrared thermography for building diagnostics, Energy Build. 34 (2) (2002) 171–183, https://doi.org/10.1016/S0378-7788(01)00105-0.

[9] E. Barreira, R.M.S.F. Almeida, M. Moreira, An infrared thermography passive approach to assess the effect of leakage points in buildings, Energy Build. 140 (2017) 224–235, https://doi.org/10.1016/j.enbuild.2017.02.009.

[10] A. Kirimtat, O. Krejcar, A review of infrared thermography for the investigation of building envelopes: advances and prospects, Energy Build. 176 (2018) 390–406, https://doi.org/10.1016/j.enbuild.2018.07.052.

[11] A. Kylili, et al., Infrared thermography (IRT) applications for building diagnostics: a review, Appl. Energy 134 (2014) 531–549, https://doi.org/10.1016/j.apenergy.2014.08.005.

[12] X.P. Maldague, et al., Detection of moisture in porous materials by infrared thermography, Thermosense XXIV (2002), https://doi.org/10.1117/12.459581.

[13] A. Atef, et al., Multi-tier method using infrared photography and GPR to detect and locate water leaks, Autom. ConStruct. 61 (2016) 162–170, https://doi.org/10.1016/j.autcon.2015.10.006.

[14] P.M. Bach, J.K. Kodikara, Reliability of infrared thermography in detecting leaks in buried water reticulation pipes, IEEE J. Sel. Top. Appl. Earth Obs. Rem. Sens. 10 (9) (2017) 4210–4224, https://doi.org/10.1109/Jstars.2017.2708817.

[15] M.H. Manekiya, P. Arulmozhivarman, Leakage detection and estimation using IR thermography, in: 2016 *International Conference on Communication and Signal Processing (ICCSP), 6-8 April 2016*, IEEE, Piscataway, NJ, USA, 2016, https://doi.org/10.1109/ICCSP.2016.7754411.

[16] B. Shakmak, A. Al-Habaibeh, Detection of water leakage in buried pipes using infrared technology; A comparative study of using high and low resolution infrared cameras for evaluating distant remote detection, in: 2015 IEEE Jordan Conference on Applied Electrical Engineering and Computing Technologies (AEECT), 3-5 Nov. 2015, IEEE, Piscataway, NJ, USA, 2015, https://doi.org/10.1109/AEECT.2015.7360563.

[17] F. Chunli, S. Fengrui, Y. Li, Investigation on nondestructive evaluation of pipelines using infrared thermography, in: 2005 Joint 30th International Conference on Infrared and Millimeter Waves and 13th International Conference on Terahertz Electronics, 2005, https://doi.org/10.1109/icimw.2005.1572551.

[18] J.X. Wu, Leakage detection method of buried heating pipelines based on soil temperature and humidity, Heat. Vent. Air Cond. 48 (9) (2018) 58–62. Available from: https://kns.cnki.net/kcms/detail/detail.aspx?FileName=NTKT201809012&DbName=CJFQ2018.

[19] Yu Xiao, Hua Yu, Qiang Lu, Gao, Pipeline image diagnosis algorithm based on neural immune ensemble learning, Int. J. Pres. Ves. Pip. 189 (2021) 303–313, https://doi.org/10.1016/j.ijpvp.2020.104249.

[20] Xiao Yu, Xuesong Tian, A fault detection algorithm for pipeline insulation layer based on immune neural network, Int. J. Pres. Ves. Pip. (2022) 196, https://doi.org/10.1016/j.ijpvp.2022.104611.

[21] S.K. Sinha, P.W. Fieguth, Segmentation of buried concrete pipe images, Autom. ConStruct. 15 (1) (2006) 47–57, https://doi.org/10.1016/j.autcon.2005.02.007.

[22] R.C. Gonzalez, R.E. Woods, Digital Image Processing, Prentice Hall, 2002, p. 793.

[23] H. Yan, Unified formulation of a class of image thresholding techniques, Pattern Recogn. 29 (12) (1996) 2025–2032, https://doi.org/10.1016/S0031-3203(96)00050-7.

[24] S.J. Wang Yongxiong, A hierarchical image segmentation method, in: Proceedings of the 31st Chinese Control Conference, 2012, pp. 1762–1767. Available from: https://kns.cnki.net/kcms/detail/detail.aspx?FileName=KZLL201207002327&DbName=IPFD2012.

[25] J. Goutsias, H.J.A.M. Heijmans, K. Sivakumar, Morphological operators for image sequences, Comput. Vis. Image Understand. 62 (3) (1995) 326–346, https://doi.org/10.1006/cviu.1995.1058.

[26] J. Serra, Introduction to mathematical morphology, Comput. Vis. Graph Image Process 35 (3) (1986) 283–305, https://doi.org/10.1016/0734-189x(86)90002-2.

[27] K. Jung, K.I. Kim, A.K. Jain, Text information extraction in images and video: a survey, Pattern Recogn. 37 (5) (2004) 977–997, https://doi.org/10.1016/j.patcog.2003.10.012.

[28] M. Ryan, N. Hanafiah, An examination of character recognition on ID card using template matching approach, in: International Conference on Computer Science and Computational Intelligence (Iccsci 2015), vol. 59, 2015, pp. 520–529, https://doi.org/10.1016/j.procs.2015.07.534.

[29] T.C. Su, et al., Morphological segmentation based on edge detection for sewer pipe defects on CCTV images, Expert Syst. Appl. 38 (10) (2011) 13094–13114, https://doi.org/10.1016/j.eswa.2011.04.116.

[30] Y.X. Wang, J.B. Su, Automated defect and contaminant inspection of HVAC duct, Autom. ConStruct. 41 (2014) 15–24, https://doi.org/10.1016/j.autcon.2014.02.001.

[31] J. Canny, A computational approach to edge-detection, IEEE Trans. Pattern Anal. Mach. Intell. 8 (6) (1986) 679–698, https://doi.org/10.1109/Tpami.1986.4767851.

[32] P. Kovesi, MATLAB and Octave Functions For Computer Vision And Image Processing, 2000 [cited 2021]. Available from: https://www.peterkovesi.com/matlabfns/.

[33] M. Sokolova, G. Lapalme, A systematic analysis of performance measures for classification tasks, Inf. Process. Manag. 45 (4) (2009) 427–437, https://doi.org/10.1016/j.ipm.2009.03.002.